www.sciencemag.org/cgi/content/full/331/6019/881/DC1

Supporting Online Material for

The Crystal Structure of the Signal Recognition Particle in Complex with Its Receptor

Sandro F. Ataide, Nikolaus Schmitz, Kuang Shen, Ailong Ke, Shu-ou Shan, Jennifer A. Doudna,* Nenad Ban*

*To whom correspondence should be addressed. E-mail: ban@mol.biol.ethz.ch (N.B.); doudna@berkeley.edu (J.A.D.)

Published 18 February 2011, *Science* **331**, 881 (2011)
DOI: 10.1126/science.1196473

This PDF file includes:

Supporting Online Material for

The Crystal Structure of the Signal Recognition Particle in Complex with its Receptor

Sandro F. Ataide, Nikolaus Schmitz*, Kuang Shen*, Ailong Ke, Shu-ou Shan, Jennifer A. Doudna†, Nenad Ban†

†To whom correspondence should be addressed. E-mail: (N.B.) ban@mol.biol.ethz.ch or (J.A.D.) doudna@berkeley.edu

* These authors have contributed equally to this work.

This PDF file includes

Materials and Methods

Protein and RNA expression and purification

Cloning of the wild type 4.5S RNA from *E.coli* and *D. radiodurans* was performed as described previously (*1*). The N-terminal truncated version of FtsY (residues 196-498) and the C-terminally truncated Ffh (residues 1-432) from *E. coli* containing an N-terminal His_6 tag were expressed and purified as described previously (*2*). The homologous and heterologous complexes were reconstituted *in vitro* by RNA refolding (*3*) followed by incubation with a 2x molar excess of purified Ffh in buffer containing (50mM Hepes pH 7.5, 150mM KOAc, 5mM $MgOAc_2$, 2mM TCEP, 0.01% Nikkol ($C_{12}E_8$), 10% (w/v) glycerol) and incubated at room temperature for 30 min. After SRP reconstitution, purified FtsY (at same molar equivalent to Ffh) was added to the reaction together with 2.5mM GMP-PCP and further incubated for 30 min at room temperature followed by an overnight incubation at 4^oC. The complex was purified using a Mono-Q column (Pharmacia) equilibrated with buffer A (50mM Hepes pH 7.5, 150mM KOAc, 5mM $MgOAc_2$, 2mM TCEP, 0.01% Nikkol, 5% (w/v) glycerol, 50µM GMP-PCP) and eluted with a gradient of Buffer B (Buffer A with 1M NaCl). The SRP:SR complex elutes around 50% of Buffer B and fractions containing the entire complex were pooled, concentrated and buffer exchanged to Buffer A supplemented with 2.5mM GMP-PCP and stored at 4^oC.

E. coli Ffh, FtsY and wild type 4.5S RNA for biochemical assays were expressed and purified as described (*15*). Truncated SRP RNAs and mutations of C86 were prepared by *in vitro* transcription, using a pSP65-derived plasmid in which an extra SacI restriction site was introduced by QuickChange mutagenesis. DNA fragments encoding the

truncated RNAs were cloned between the PstI and SacI sites behind the T7 promoter. Plasmids containing truncated SRP RNAs were digested with SacI for run-off transcription by T7 polymerase (Ambion Megascript). The RNAs were allowed to fold during transcription, isolated by acid phenol extraction, and further purified by gel filtration chromatography on TSK3000. Only the peaks corresponding to the monomeric species (Table S2) were used for activity assays. All the truncated RNAs were confirmed by MALDI-TOF to have the correct molecular weight.

Crystallization conditions and structure determination

Crystals of the purified homologous complex grew under vapor diffusion at 19^{o}C in sitting drops. 0.5µL of the complex solution (8 mg/mL) was mixed with 0.5µL of the well solution containing 16% PEG 3350, 210mM LiCl, 5mM $MgOAc_2$, 5% (w/v) glycerol, in 50 mM MES pH 6.7. Crystals were observed after 4 days and harvested after 2 weeks incubation. Well solution containing 25% glycerol was used as a cryo-protectant. Crystals of the purified heterologous complex grew under vapor diffusion at 19^{o}C in sitting drops. 1µL of the complex solution (7mg/mL) was mixed with 1µL of the well solution containing 12% PEG 2000 MME, 260mM LiCl, 50mM $MgOAc_2$, 11% (w/v) glycerol, in 50 mM Bis-Tris pH 6.9. Crystals were observed after 4 days and harvested after 2 weeks incubation. Well solution containing 25% glycerol was used as a cryo-protectant. Data of the heterologous complex was collected on the Beamline X06SA of the Swiss Light Source, PSI, Villigen and the data of the homologous were collected on Beamlines 8.2.2 of Advanced Light Source, Lawrence Berkeley National Laboratory. Data reduction and scaling were carried out using the XDS package (*4*). The structure of

the heterologous complex was solved at a resolution of 3.9Å by molecular replacement with PHASER (*5*) using available high-resolution structures of the Ffh-FtsY NG heterodimer and the Ffh M-domain and the tetraloop region of 4.5S RNA (PDB identifier 1RJ9 and 1HQ1, respectively). The model was built using iterative rounds of model building in COOT (*6*) and ONO (*7*) and refinement with AutoBuster 2.4 (*8*) and CNS1.3 (*9, 10*). 2-fold local similarity symmetry restraints (LSSR) as implemented in AutoBuster or 2-fold NCS have been applied in all refinements. For model building and representation, B-factor sharpening and softening according to the local signal to noise ratio of the electron density was applied (between -80 and +20Å^2). The bound GTP analogues were refined as single rigid bodies, due to the intermediate resolution of the structure (GMPPCP coordinates taken from PDB ID 2cnw). Canonical RNA base-pair hydrogen bonds were restrained during the refinement by manually setting up corresponding distance restraints for CNS or AutoBuster. Inspection of the overall B-factor distribution indicates that one NG dimer and the M-domain tetraloop region of the respective other molecule in the ASU are better ordered, which can be explained by the observed crystal packing. Moreover the smallest thermal motion is observed for the GTPase centers of the NG-dimers, while peripheral, solvent exposed regions show higher B-factors. Intrinsic flexibility of the complex mainly through interdomain movements (as indicated by high contribution of the TLS tensors to the overall B-factors) is observed, resulting in high overall B-factors.

The datasets of the heterologous and homologous complexes are isomorphous (weighted cross R-factor: 6.1 %, overall correlation 0.87, calculated using SCALEIT and phenix.reflection_statistics, respectively)(*11, 12*). A rigid body refinement of the

coordinates of the heterologous complex against the data of the homologous complex in AutoBuster 2.4 resulted in R_work/R_free: 33.6/33.9 and yielded interpretable maps at 7 Å. The electron density maps confirmed that the homologous and the heterologous complexes share the same overall structure. Additional density at the 5',3' end of the *E. coli* SRP RNA representing additional nucleotides of the larger *E. coli* SRP RNA is observed.

An omit map for the Ffh linker (residues 300-330) and the SRP RNA tetraloop (residues 47-54) shows clear difference densities for both regions (Figure S1).

All figures are generated with Pymol (*13*). Surface area interaction was calculated with PISA (*14*). For the generation of all figures the better ordered molecule of the heterologous complex in the crystal was used.

GTPase activity

Measurements of the stimulated GTPase reaction between SRP and FtsY were carried out as described previously (*15, 16*). Briefly, reactions were carried out in SRP buffer [50 mM KHEPES, pH 7.5, 150 mM KOAc, 2 mM $Mg(OAc)_2$, 2 mM DTT, 0.01% Nikkol] in the presence of a small, fixed amount of SRP (50–100 nM) or Ffh (500 nM), varying amounts of FtsY, and saturating GTP (100 – 200 μM). The observed rate constants (k_{obsd}) were fit to Eq. 1,

$$k_{obsd} = k_{cat} \times \frac{[\mathrm{SR}]}{K_m + [\mathrm{SR}]} \qquad (1)$$

in which k_{cat} is the maximal rate constant at saturating FtsY concentrations, and K_m is the concentration required to reach half saturation. Because k_{cat} is at least 100-fold faster than the rate of SRP:FtsY complex disassembly, the rate constant k_{cat}/K_m in this assay is

rate-limited by and therefore equal to the rate of stable SRP-FtsY complex formation (*15*), and the value of k_{cat} represents the rate of GTP hydrolysis or a rate-limiting conformational change preceding GTP hydrolysis.

Fluorescence experiments

Ffh-C235 was labeled with acrylodan (Invitrogen) and purified as described (*16*). Fluorescence measurements were carried out on a FluoroLog-3-22 spectrofluorometer (Jobin-Yvon, Edison, NJ) in SRP buffer. Association rate constants for GTP-dependent SRP-FtsY complex formation were determined by mixing 50 – 100 nM acrylodan-labeled Ffh-C235 (bound to wildtype or mutant SRP RNAs) with varying amounts of FtsY in the presence of 100 μM GppNHp and monitoring the time course of fluorescence change. Linear fits of observed rate constants as a function of FtsY concentration ($k_{obsd} = k_{on}$ [FtsY] + k_{off}) gave the second-order association rate constant k_{on}.

Table S1. Summary of crystallographic data

Crystal form	SRP:SR complex (*D.radiodurans* RNA)	SRP:SR complex (*E.coli* RNA)
Space group	$P2_12_12_1$	$P2_12_12_1$
Unit cell dimensions		
a, b, c (Å)	84.10, 131.04, 266.04	86.13, 131.38, 266.87
α, β, γ (˚)	90, 90, 90	90, 90, 90
Data collection		
Wavelength (Å)	1.0	1.0
Resolution (Å)[a]	49.0 - 3.94 (4.17 - 3.94)	25.0 – 7.0 (7.42 – 7.01)
Unique reflections	26790	5100
Redundancy [a]	2.5 (2.5)	6.8
Completeness (%)[a]	94.0 (95.3)	99.2 (97.2)
R_{meas} (%)[a]	4.8 (84.0)	12.8 (41.0)
I/σ(I)[a]	12.9 (1.6)	14.3 (3.9)
Model statistics		
Refinement		
Nonhydrogen atoms	15088	
Protein	10570	
Ligand/ion	4518	
B-factor overall	227.7	
Protein	220.0	
Ligand/ion	183.1	
Resolution (Å)	45.79 - 3.94	
R_{work}/R_{free} (%)	23.4/26.8	
Number of test reflections	1281	
RMS deviations		
Bonds (Å)	0.008	
Angles (˚)	1.08	

[a] Values for highest resolution shells are given in parentheses

Table S2. Elution volume of wildtype and mutant SRP RNAs during size-exclusion chromatography on TSK3000.

RNA Species	Monomer Elution Volume (mL)
wt 4.5S RNA (114mer)	115.4
tRNA (74mer)	131.9
100mer	119.8
92mer	123.6
82mer	127.1
68mer	135.0
56mer	144.9
43mer	142.6

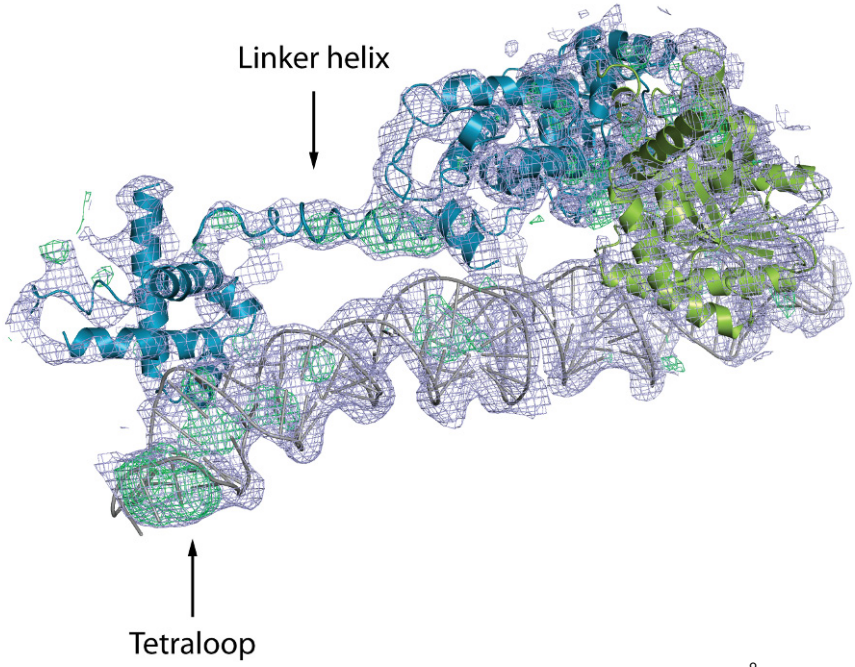

Fig. S1. Electron density maps for the E. coli SRP SR complex at 7 Å. 2 F_{obs}-F_{calc} electron density map shown in light blue (contour level 1.0 σ). Unbiased omit maps for the linker region and the tetraloop (F_{obs}-F_{calc}, green mesh) is contoured at 2.5 σ. Maps were calculated after one round of rigid body refinement using the coordinates of heterologous complex with occupancies for the linker region and the tetraloop set to 0. For clarity maps were carved with a radius of 5 Å using pymol.

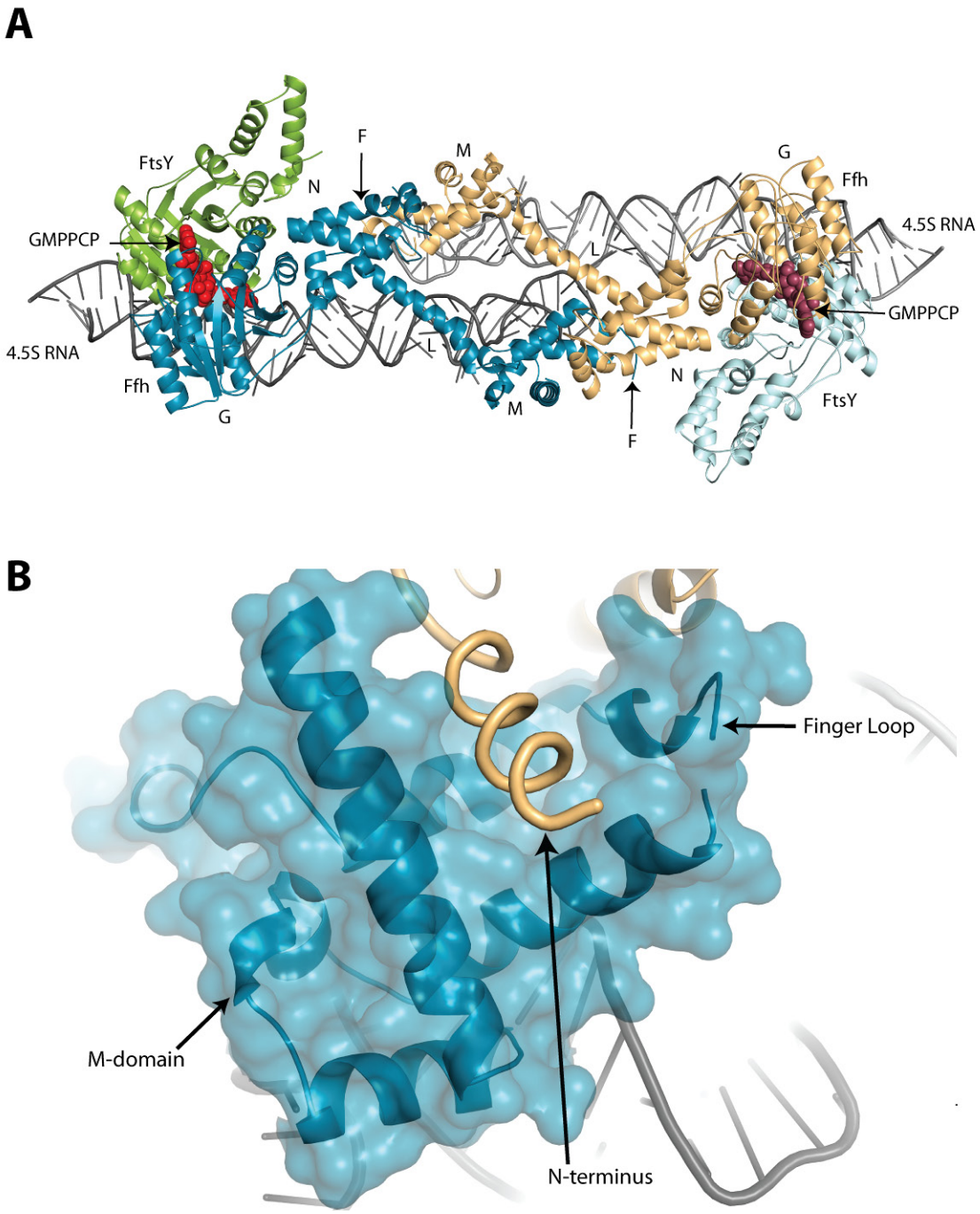

Fig S2. **Arrangement of the SRP:SR complex in the asymmetric unit with showing the interaction of the Ffh N-terminal domain with NCS related Ffh M-domain. (A)** Arrangement of the NCS related molecules in the asymmetric unit for the SRP:SR complex. Ffh is colored in blue, 4.5S RNA in gray, FtsY (SR) is shown in green for one

copy and Ffh is colored in cyan, 4.5S RNA in light gray, FtsY is shown in gold. The atoms of the two GMP-PCP molecules per complex are displayed as red or burgundy spheres. N corresponds to N-terminal domain, G is the GTPase domain, M is the M-domain and L is the flexible linker, F is part of the finger loop. **(B)** The bound conformation of the M-domain encloses an N-terminal helix of the NCS related Ffh. The surface and cartoon representation of Ffh M-domain and the observed parts of the finger loop (residues 358-366 not build) is displayed in blue with N-terminal helix form the NCS Ffh displayed as a tube cartoon in golden and the 4.5S RNA in gray.

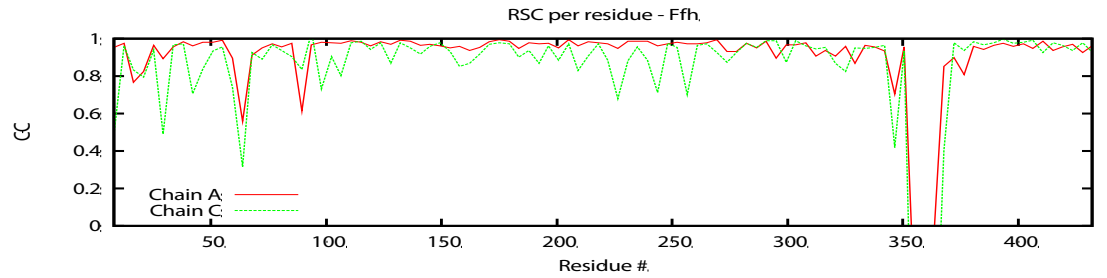
RSC per residue - Ffh
CC
Chain A
Chain C
Residue #

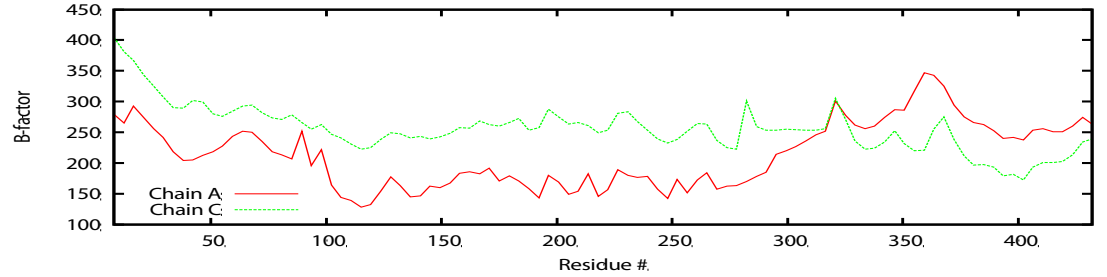
B-factor
Chain A
Chain C
Residue #

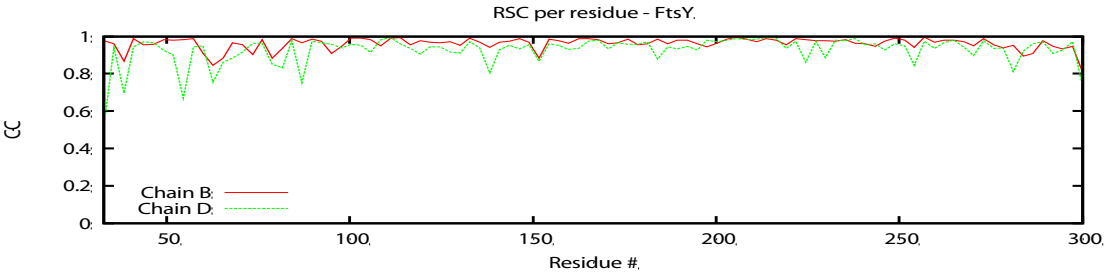
RSC per residue - FtsY
CC
Chain B
Chain D
Residue #

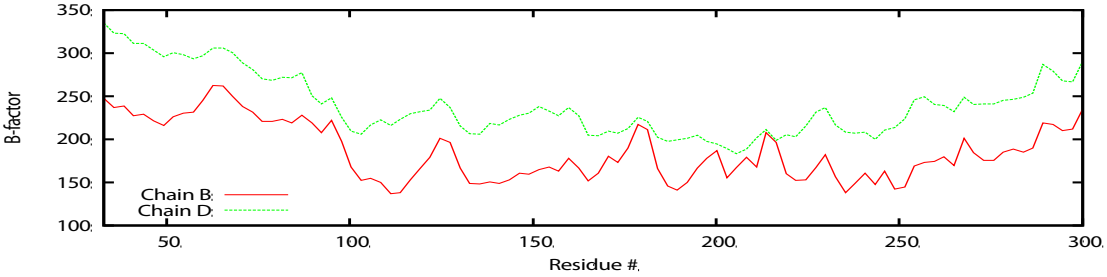
B-factor
Chain B
Chain D
Residue #

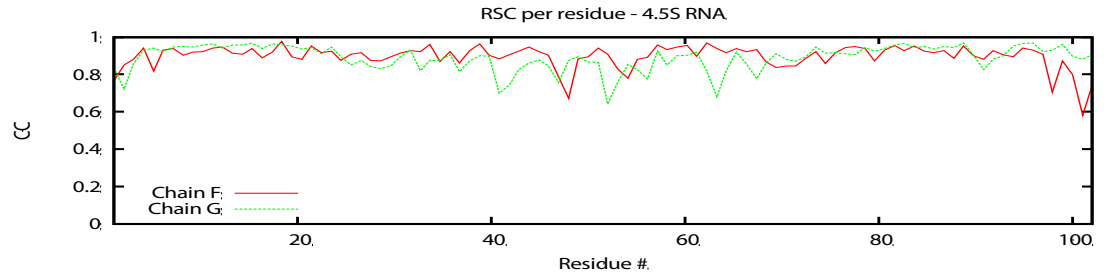
RSC per residue - 4.5S RNA
CC
Chain F
Chain G
Residue #

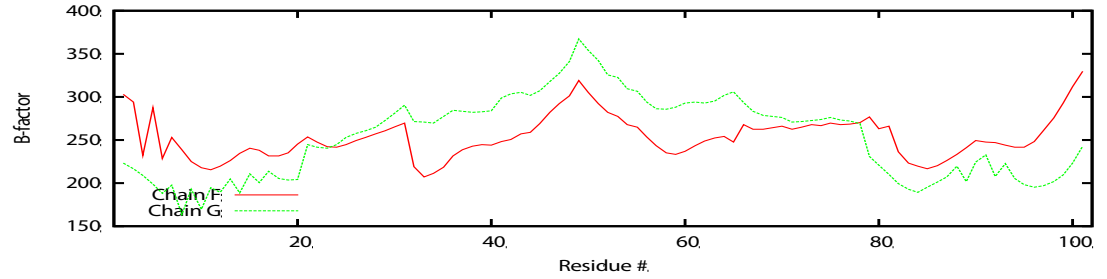
B-factor
Chain F
Chain G
Residue #

Fig. S3. Real space cross-correlation between $2mF_o$-DF_c and F_c maps and B-factor distribution for both complexes in the asymmetric unit. Plot shows cross correlation and B-factor per residue. The twin NG domains and the distal part of the RNA of SRP exhibit lower B-factors, while the M domain and the tetraloop are less defined. This is especially pronounced for the side chains in the finger loop region in the M domain (Chains A and C, residues 343-368). Real space cross-correlation has been computed using the Phenix model_vs_data module. Plots were generated using Gnuplot (PHENIX version 1.6.1).

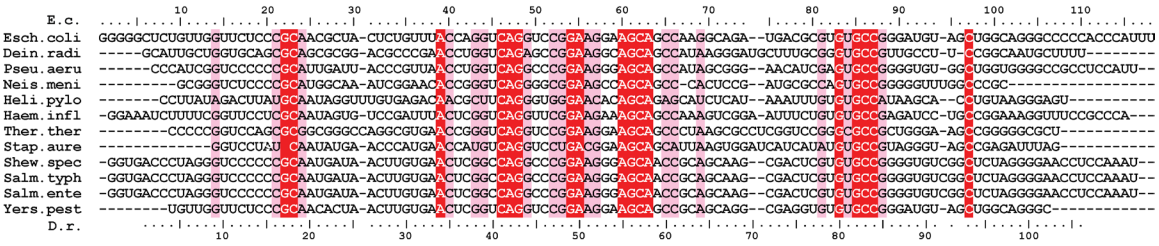

Fig S4. Conservation of 4.5S RNA. Alignment of 4.5S RNA with >95% conserved residues indicated in red and residues with >75% conservation indicated in light pink. *E.coli* numbering indicated on top and *D. radiodurans* numbering indicated on the bottom.

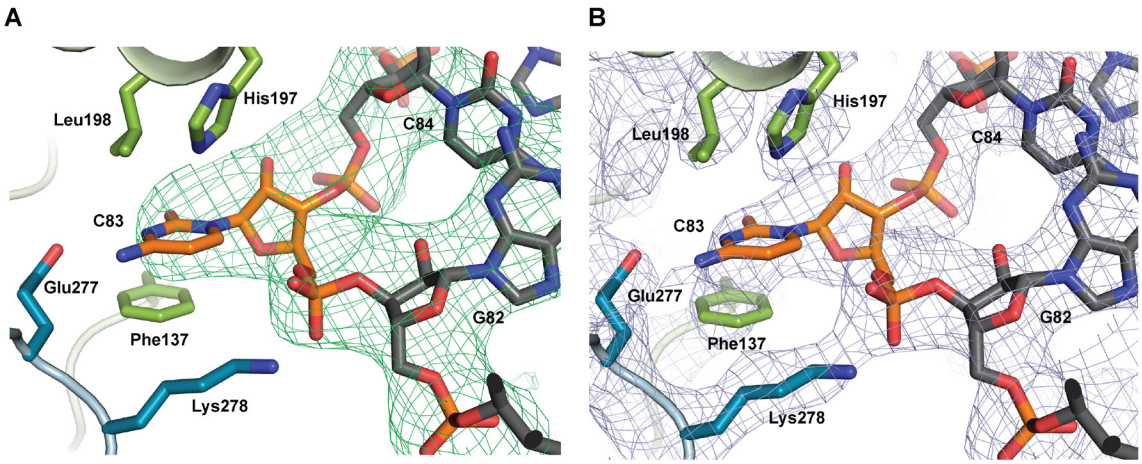

Fig. S5. Electron density maps for the nucleotide binding region. **(A)** Unbiased F_{obs}-F_{calc} omit map for bases C82 to G84 shown as green mesh countered at 2.5σ. The flipped out orientation of the unpaired base can be unambiguously identified. **(B)** 2 F_{obs}-F_{calc} electron density map for the nucleotide binding region shown as blue mesh. Map is countered at 1.0 σ and B-sharpened by -60$Å^2$. Most side chains can be placed unambiguously.

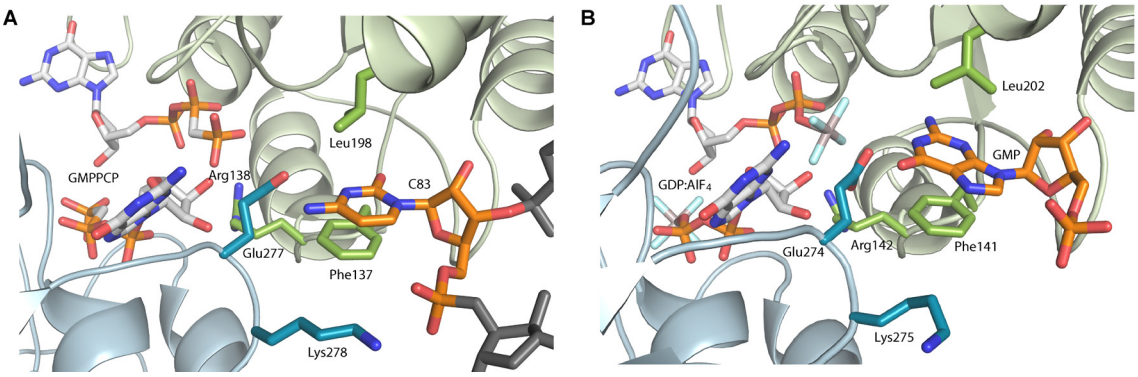

Fig. S6. Comparison between SRP:SR NG domain interacting with a conserved flipped base at 5'-3' distal end of the 4.5S RNA or and external GMP. (A) Close-up view of the interaction of the conserved flipped C83 with the interface of Ffh and FtsY . 4.5S RNA is displayed as sticks colored in gray with C83 colored in orange. Ffh (blue) and FtsY (green) residues that interact directly with C83 are displayed as sticks. GMP-PCP residues are represented as sticks colored with white carbons, red oxygens, blue nitrogens and orange phosphates. **(B)** Close up view of the external nucleotide binding site of Ffh:FtsY NG domain from *T.aquaticus* (PDB 2cnw)(*17*) and GDP:AlF_4. GMP is colored and displayed as base C83 in (**A**). GDP:AlF_4 residues are represented as sticks colored with white carbons, red oxygens, blue nitrogens, orange phosphates, cyan fluorines and grey aluminium.

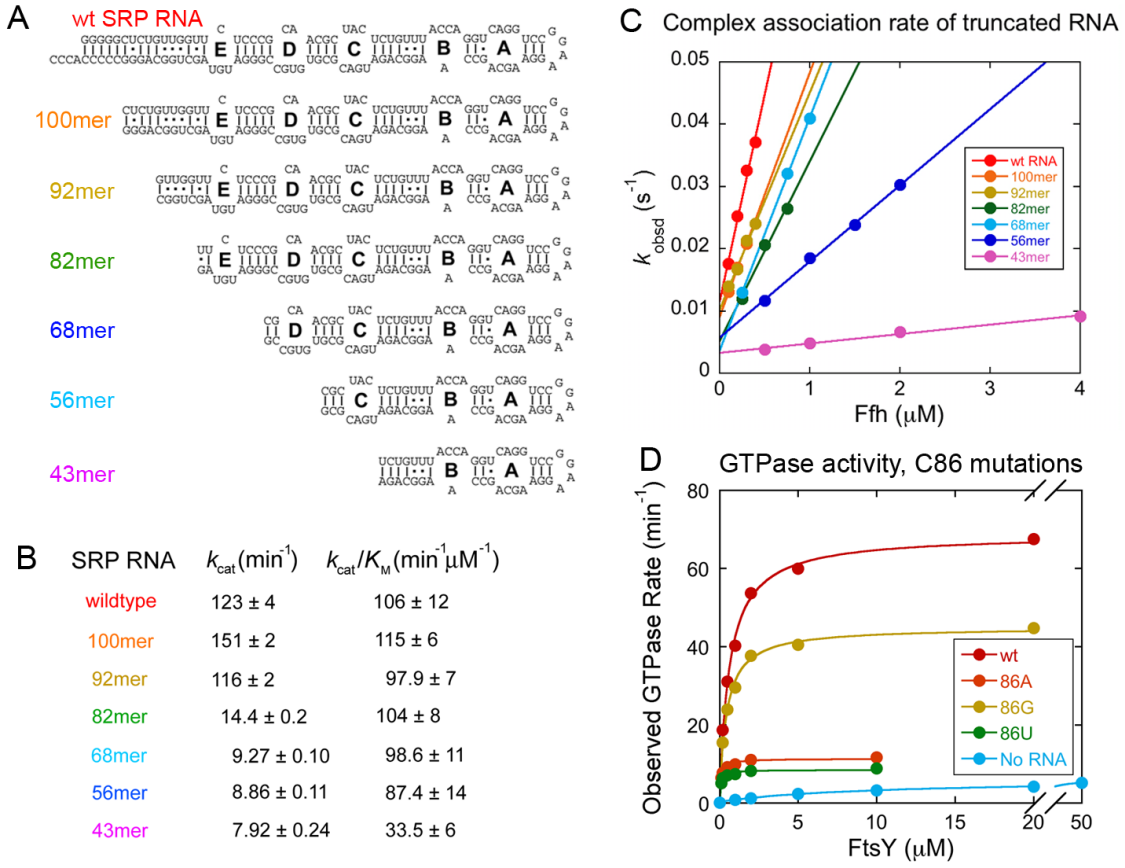

B

SRP RNA	k_{cat} (min^{-1})	k_{cat}/K_M ($min^{-1}\mu M^{-1}$)
wildtype	123 ± 4	106 ± 12
100mer	151 ± 2	115 ± 6
92mer	116 ± 2	97.9 ± 7
82mer	14.4 ± 0.2	104 ± 8
68mer	9.27 ± 0.10	98.6 ± 11
56mer	8.86 ± 0.11	87.4 ± 14
43mer	7.92 ± 0.24	33.5 ± 6

Fig. S7. **(A)** *E. coli* SRP RNA systematically truncated from the distal end that were used in this study. **(B)** Summary of the rate constants derived from the data in Figure 4B. **(C)** Observed rate constants of SRP-FtsY complex formation ($k_{obsd} = k_{on}$ [FtsY] + k_{off}) were determined for the wild type and mutant SRP RNAs using fluorescence assays. Linear fits of the data gave complex formation rate constants (k_{on}) of 4.58×10^4, 3.90×10^4, 3.48×10^4, 2.88×10^4, 3.74×10^4, 1.22×10^4, and 1.51×10^3 $M^{-1}s^{-1}$ for wild type SRP RNA and for the 100mer, 92mer, 82mer, 68mer, 56mer, and 43mer RNAs, respectively. **(D)** Stimulated GTPase activity between SRP and FtsY with mutations in SRP RNA C86. The data were fit to the Michaelis-Menten equation, and the relative values of k_{cat} are summarized in Figure 4E.

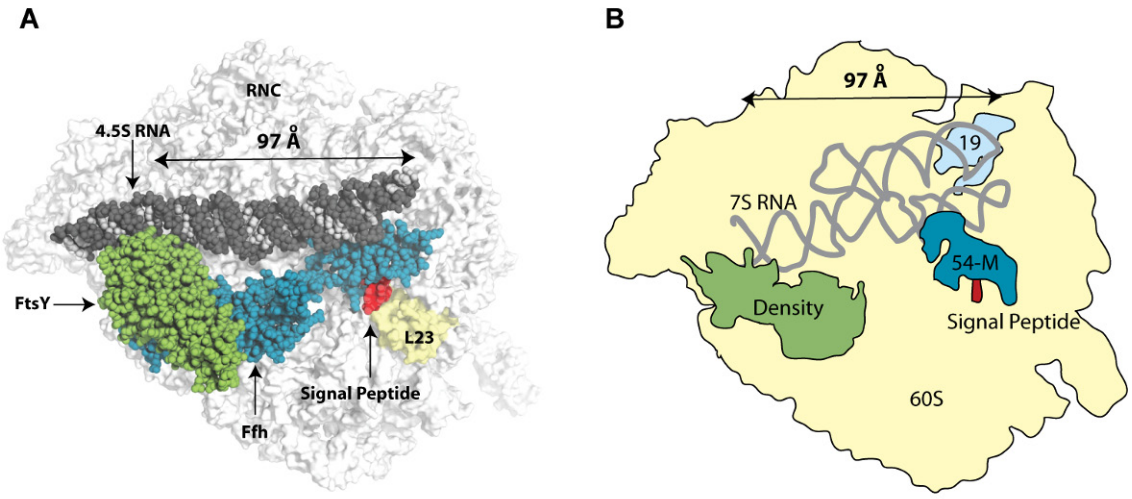

Fig. S8. Conformation of the prokaryotic and eukaryotic SRP:SR structure on the ribosome. (A) The SRP receptor complex in the cargo release conformation modeled on the ribosome is compared to the cartoon representation of the eukaryotic RNC:SRP:SR complex reconstruction (*18, 19*). **(B)** SRP54 M-domain is colored blue (54-M) the 7S RNA S-domain in gray, signal peptide as red, SRP19 (19) in light blue. Additional density observed in the distal region of the 7S SRP RNA may originate from the repositioned heterodimeric NG domains rather than the SRP receptor alpha and beta as suggested (*18*). The distance between tetraloop and C84 for SRP:SR and the tetraloop of Helix 8 and the 5',3'-distal portion oh Helix 5 of the 7S RNA are the same and indicated in the figure.

References

1. R. T. Batey, M. B. Sagar, J. A. Doudna, Structural and energetic analysis of RNA recognition by a universally conserved protein from the signal recognition particle. *J Mol Biol* **307**, 229 (Mar 16, 2001).
2. R. J. Spanggord, F. Siu, A. Ke, J. A. Doudna, RNA-mediated interaction between the peptide-binding and GTPase domains of the signal recognition particle. *Nat Struct Mol Biol* **12**, 1116 (Dec, 2005).
3. F. Y. Siu, R. J. Spanggord, J. A. Doudna, SRP RNA provides the physiologically essential GTPase activation function in cotranslational protein targeting. *RNA* **13**, 240 (Feb, 2007).
4. W. Kabsch, Xds. *Acta Crystallogr D Biol Crystallogr* **66**, 125 (Feb, 2010).
5. A. J. McCoy *et al.*, Phaser crystallographic software. *J Appl Crystallogr* **40**, 658 (Aug 1, 2007).
6. P. Emsley, B. Lohkamp, W. G. Scott, K. Cowtan, Features and development of Coot. *Acta Crystallogr D Biol Crystallogr* **66**, 486 (Apr, 2010).
7. G. J. Kleywegt, T. A. Jones, Software for handling macromolecular envelopes. *Acta Crystallogr D Biol Crystallogr* **55**, 941 (Apr, 1999).
8. E. Blanc *et al.*, Refinement of severely incomplete structures with maximum likelihood in BUSTER-TNT. *Acta Crystallogr D Biol Crystallogr* **60**, 2210 (Dec, 2004).
9. A. T. Brunger, Version 1.2 of the Crystallography and NMR system. *Nat Protoc* **2**, 2728 (2007).
10. G. F. Schroder, M. Levitt, A. T. Brunger, Super-resolution biomolecular crystallography with low-resolution data. *Nature* **464**, 1218 (Apr 22, 2010).
11. The CCP4 suite: programs for protein crystallography. *Acta Crystallogr D Biol Crystallogr* **50**, 760 (Sep 1, 1994).
12. P. D. Adams *et al.*, PHENIX: a comprehensive Python-based system for macromolecular structure solution. *Acta Crystallogr D Biol Crystallogr* **66**, 213 (Feb, 2010).
13. L. Delano-Wood. (DeLano Scientific LLC, 2008).
14. E. Krissinel, K. Henrick, Inference of macromolecular assemblies from crystalline state. *J Mol Biol* **372**, 774 (Sep 21, 2007).
15. P. Peluso, S. O. Shan, S. Nock, D. Herschlag, P. Walter, Role of SRP RNA in the GTPase cycles of Ffh and FtsY. *Biochemistry* **40**, 15224 (Dec 18, 2001).
16. X. Zhang, C. Schaffitzel, N. Ban, S. O. Shan, Multiple conformational switches in a GTPase complex control co-translational protein targeting. *Proc Natl Acad Sci U S A* **106**, 1754 (Feb 10, 2009).
17. P. J. Focia, J. Gawronski-Salerno, J. S. t. Coon, D. M. Freymann, Structure of a GDP:AlF4 complex of the SRP GTPases Ffh and FtsY, and identification of a peripheral nucleotide interaction site. *J Mol Biol* **360**, 631 (Jul 14, 2006).
18. M. Halic *et al.*, Signal recognition particle receptor exposes the ribosomal translocon binding site. *Science* **312**, 745 (May 5, 2006).
19. M. Halic *et al.*, Following the signal sequence from ribosomal tunnel exit to signal recognition particle. *Nature* **444**, 507 (Nov 23, 2006).